ISSN 1070-3632, Russian Journal of General Chemistry, 2013, Vol. 83, No. 11, pp. 2173–2181. © Pleiades Publishing, Ltd., 2013.
Original Russian Text © N.I. Kiselev, D.A. Velikanov, S.B. Korchagina, E.A. Petrakovskaya, A.D. Vasil'ev, L.A. Solov'ev, D.A. Balaev, O.A. Bayukov, I.A. Denisov, S.S. Tsegel'nik, E.V. Eremin, D.A. Znak, K.A. Shaikhutdinov, A.A. Shubin, N.P. Shestakov, N.V. Volkov, S.K. Gordeev, P.I. Belobrov, 2012, published in Rossiiskii Khimicheskii Zhurnal, 2012, Vol. 56, Nos. 1–2, pp. 50–57.

Electrical and Magnetic Properties of Nanodiamond and Pyrocarbon Composites

N. I. Kiselev[a], D. A. Velikanov[a], S. B. Korchagina[b], E. A. Petrakovskaya[a], A. D. Vasil'ev[a], L. A. Solov'ev[c], D. A. Balaev[a], O. A. Bayukov[a], I. A. Denisov[d], S. S. Tsegel'nik[d], E. V. Eremin[a], D. A. Znak[d], K. A. Shaikhutdinov[a], A. A. Shubin[d], N. P. Shestakov[a], N. V. Volkov[a], S. K. Gordeev[b], and P. I. Belobrov[d]

[a] *Kirenskii Institute of Physics, Siberian Branch, Russian Academy of Sciences, Akademgorodok 50, str. 38, Krasnoyarsk, 660036 Russia*

[b] *Central Research Institute of Materials Federal Unitary Enterprise, St. Peterburg, Russia*

[c] *Institute of Chemistry and Chemical Technology, Siberian Branch, Russian Academy of Sciences, Krasnoyarsk, Russia*

[d] *Siberian Federal University, Youth Open Laboratory of Perspective Research and Technology, Institute of Biophysics, Siberian Branch, Russian Academy of Sciences, Krasnoyarsk, Russia*
e-mail: pe-ter.belobrov@gmail.com

Received June 1, 2012

Abstract—The electrical and magnetic properties of the nanodiamond composites comprising nanodiamond, pyrolytic carbon, and nanosized pores were studied. The composites are *p*-type semiconductors and their resistance decreases by 12 orders of magnitude as the pyrocarbon-to-diamond ratio γ increases from 0 to 80 wt %. Evidence for paramagnetic properties of the nanodiamond composites was obtained. The observed properties are explained by increased concentration of surface Tamm states. The paramagnetic properties are explained in terms of the electron spins localized on the nanodiamond surface in the composite.

DOI: 10.1134/S1070363213110376

Nanodiamond–pyrocarbon composites (NDCs) have been developed and synthesized at the Central Research Institute of Materials Federal Unitary Enterprise (St. Petersburg) [1–3]. Over more than 10 years experimental research on the electrical and magnetic susceptibility of NDC materials has been performed. The experimental results have been discussed in [4–17]. It the present paper we provide a generalized view of the electrical and magnetic properties of NDCs.

Structure and Principal Characteristics of NDCs

In NDCs, individual nanodiamond particles are linked to pyrocarbon. The most part of carbon atoms in the pyrocarbon matrix (graphene flakes) are present in the sp^2-hybridized state, whereas the carbon atoms forming the diamond phase are sp^3-hybridized. A characteristic feature of this carbon material is its high open porosity.

Thus, NDCs combine three types of interlinked nanofragments: nanodiamonds, nanosized graphite-like matrix, and nanopores (Fig. 1).

Nanodiamonds are present as 3D-ordered particles with an average size of about 4–5 nm. The small thickness of the pyrocarbon matrix allows it to be considered as a 2D system on the nanoscale. On the microscale, the three phases form a 3D core which endows the composites with sufficient strength and favors preservation of the preset 3D shape.

Unlike what is observed with nanodiamonds, the X-ray pattern of NDCs is fairly well defined, and even the reflexes at 400 and 133 are evident (Fig. 2).

We performed independent measurements to show that all the obtained dependences of diffraction intensities allow estimation of the size of coherent scattering regions.

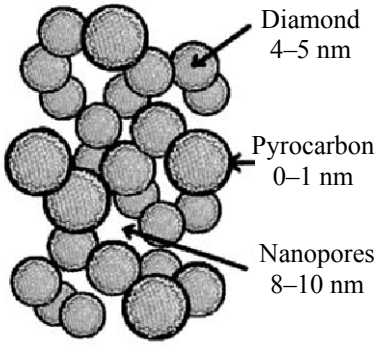

Fig. 1. Structure of a NDC composite.

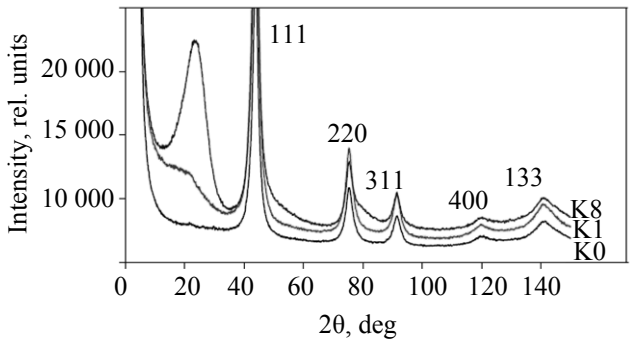

Fig. 2. X-ray patterns of NDCs with different pyrocarbon weight fractions γ. Sample, γ (%): K0, 0; K1, 10; and K8, 80.

EXPERIMENTAL

The goal of the research was to find out the mechanism of electrical conductivity of NDC composites, because there were no grounds to suggest existence of an electroconductive graphite layer on the dielectric carbon surface. Special consideration should also be given to the formation of an electroconductive carbon layer on the diamond–pore phase interface.

The NDC samples containing from 0 to 80 mol% of pyrocarbon were studied. In addition, the properties of nanocomposites in which nanodiamond was replaced by aerosil ($NCSiO_2$) of the same dispersity (γ = 20%, sample NC20), as well as a composite comprising micron-sized pyrocarbon and diamond DCC (γ =10%, sample M10).

Table 1. Parameters of the temperature dependence of electrical conductivity for a nanodiamond−pyrocarbon semiconductor[a]

γ, %	ρ_{290}, Ω m	E_a, eV	E_σ, eV	B
0	1.2×10^9		~ 0.314	
0.5	8.2×10^6	0.287	0.311	
5	9.2×10^4	0.227	0.248	
10	574	0.155	0.173	62
20	1.55	0.082	0.101	40
30	0.096	0.051	0.069	24
40	0.015	0.033	0.052	17

[a] (γ) Weight fraction of pyrocarbon; (ρ_{290}) specific resistance at T = 290 K; (E_a) activation energy of electrical conductance. The values of the parameters were calculated by the following equations: E_a: $\sigma = \sigma_0\exp(-E_a/kT)$ at σ_0 = const; E_σ: $\sigma = (\sigma_m/T) \times \exp(-E_\sigma/kT)$, $\sigma_m = 8.6\times10^5$ cm/m for all samples at $E_\sigma = 0$ and T = 290; and B: $\sigma \sim A\exp(-B/T^{1/4})$ [10].

Electrical conductivity of NDCs

Temperature Dependence

The temperature dependences of the bulk conductivity of the NDCs studied (Fig. 3) are typical of semiconductors, specifically narrow-band amorphous semiconductors [18–20]. However, instead of the valence band and conductivity band, which are characteristic of classical semiconductors, NDC materials show a 1D and a 2D bands of surface electronic states [21]. The occupancy of these states, their mutual arrangement on the energy scale, and the energy gap between them can hardly be determined from the temperature dependence of the bulk NDC conductivity in the electrostatic field.

Nanodiamond–pyrocarbon composites contain no free-electron gas, unlike solid metals and semiconductors. Therefore, we suggested that the Fermi level is located in the middle of the forbidden band between the 1D and 2D bands of surface electronic states.

Electrons inside each particle are only slightly localized, since the de Broglie wavelength is comparable to the diamond particle size. The activation energies of hopping conductivity σ in NDCs, estimated from the σ(T) dependences (Fig. 3) are 0.03–0.3 eV (Table 1). The low-temperature bulk NDC conductivity is described by the Mott equation for amorphous semiconductors [18–20] (see the insert in Fig. 3, where the $\log\sigma = f(T^{-1/4})$ dependence is linear in the range 200–4 K).

Conductivity Type

The fact that the bulk NDC conductivity changes by 12 orders of magnitude as the weight fraction of pyrocarbon changes from 0 to 80% gives no grounds to

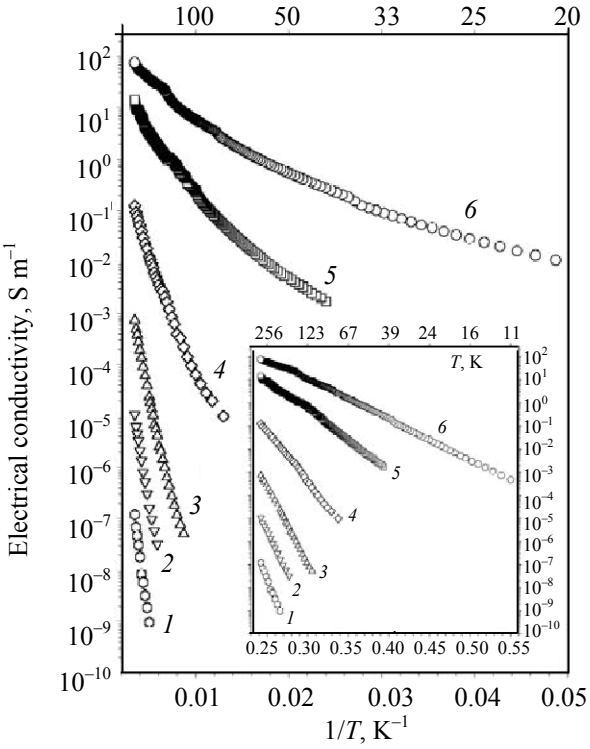

Fig. 3. Temperature dependence of electrical conductivity for semiconductor quantum dots with different pyrocarbon weight fractions γ, %: (*1*) 0.5; (*2*) 5; (*3*) 10; (*4*) 20; (*5*) 30, and (*6*) 40 [10].

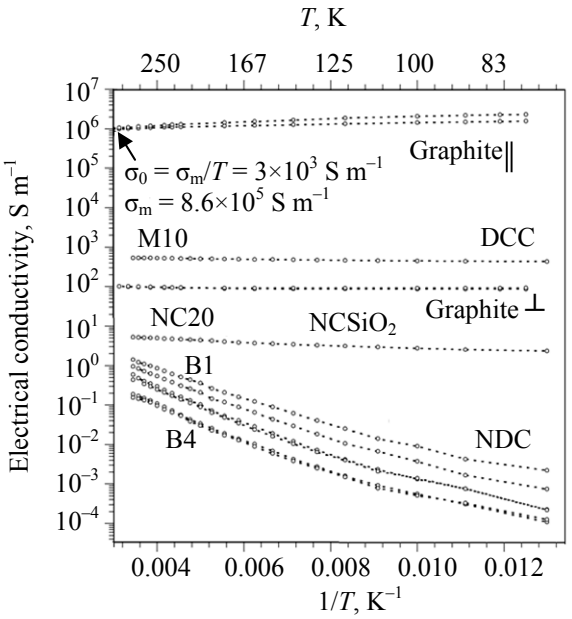

Fig. 4. Temperature dependence of specific electrical conductivity for composites on the basis of diamond and pyrocarbon (NDC, samples B1 and B4; DCC, sample M10) and on the basis of aerosil and pyrocarbon ($NCSiO_2$, sample NC_2O) in comparison with the electrical conductivity of graphite along (∥) and across (⊥) graphene layers.

suggest a metal–dielectric transition in NDCs. The physical underground of this phenomenon is still to be understood.

As seen from the data in Table 2, the thermal EMF of an NDC material has a positive sign, and the material is a *p*-type semiconductor. As references we used copper samples with similar dimensions and a negative thermal EMF of the hot end.

Influence of the Composite Type on Its Conductivity

The conductivity of NDCs was compared with the conductivity of graphite along and across the graphene layers (Fig. 4).

The experimental data in Fig. 4 provide a unique evidence showing that it is just nanodiamond and its electronic vibrational properties that are responsible for the semiconductor-type temperature dependence of conductivity. This is easily verifiable by a comparison of the specific conductivities of composites B1, B2, B3, and B4, which contain nanodiamond (~5 nm), and any other composites, for example, composites $NCSiO_2$ in which diamond is replaced by aerosil of the same dispersity (γ = 20%, sample NC20), as well as composite DCC which comprises microsized pyrocarbon and diamond (γ =10%, M10).

Note that in Figs. 3 and 4 we present different but overlapping temperature ranges.

Forbidden Band

The width of the forbidden band was estimated from the IR spectra by a commonly accepted procedure. Figure 5 shows the baselines of the IR absorption spectra for a model series of nanocomposite samples (K0–K8). (Detailed analysis of energy-derivative functions is omitted here in view of the limited volume of the present publication).

Table 2. Thermal EMFs of NDC samples [10]

Sample	γ, %	Thermal EMF, μV/K
NDC20 #B4	17.4	6.6 ± 0.2
NDC20 #B3	19.0	6.5 ± 0.6
NDC30 #Q	29.5	5.6 ± 0.1
NDC30 #P[a]	29.5	6.3 ± 0.2

[a] Sample NDC30 #P is sample NDC30 #Q (thickness ~1 mm) with layers of about ~500 μm thick removed from its both sides.

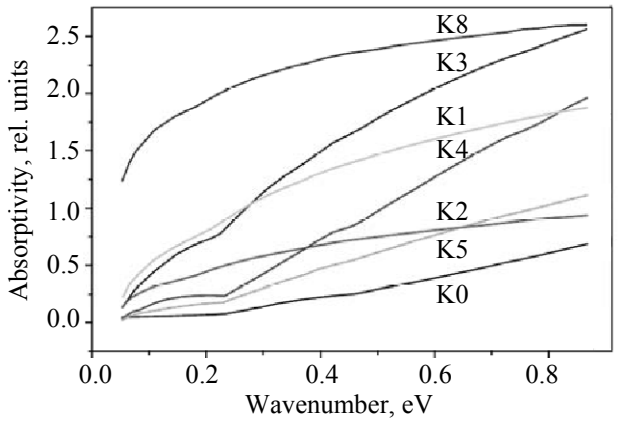

Fig. 5. Baselines of the IR spectra in the range from 500 cm^{-1} (0.057 eV) to 7000 cm^{-1} (0.79 eV) for NDCs with different pyrocarbon weight fractions γ. Sample, γ (%): K0, 0; K1, 10; K2, 20; K3, 30; K4, 40; K5, 50; and K8, 80.

As follows from Fig. 5, the characteristic energy changes which essentially affect baseline derivatives fall in the range from 50 meV to 0.45 eV, which is fairly well consistent with the activation energies of hopping conductivity, listed in Table 1. In the low-energy range and at increased pyrocarbon concentrations, the width of the forbidden band decreases. Thus, there are further grounds to suggest that NDC materials are semiconductors with a narrow forbidden band.

Sign and Mobility of Charge Carriers

The Ohm law is valid for NDCs if the current or applied voltage changes no less than 4 orders of magnitude, until to critical electric field strengths (~1 V cm^{-1}) and current density ~0.1 A cm^{-2} are reached [10].

The Hall potential and magnetic resistance change at magnetic field strengths of up to 25 kOe. At the current and voltage sensitivities of the instrument of 10^{-6} A and 10^{-7} V, respectively, these values for all the samples are equal to zero. It is hardly possible to measure mobility of charge carriers in NDCs in the Hall field, the more so as, according to recent findings, NDCs feature a spin Hall effect, like graphene, rather than a charge Hall effect.

Actually, the Hall effect can be detected at the current sensitivity of 10^{-8}A and voltage sensitivity of 10^{-9} V, but the standard measurement technique, when the direction of the magnetic field of a strength of 90 Oe is changed at a rate of 177 Oe s^{-1} does not work with NDCs. The slow magnetization reversal is probably associated with a reorientation of the collective Tamm electron in each diamond particle.

Note that we managed to observe polarity reversal of charge carriers, when the paramagnetic moment of Tamm electrons became comparable to the ferromagnetic moment of admixtures (This experiment will be described in detail after completion of measurements for the entire series of samples. Here we mention this effect as the first evidence of quantum effects in NDCs.)

Magnetic Properties of NDCs

The research on the magnetic properties of nanodiamond–pyrocarbon composites involved assessment of the ability of these materials for magnetic ordering and their principal magnetic characteristics: magnetic susceptibility, temperature and field dependences of magnetization, type of magnetic order, magnetic resonance parameters (NMR, ESR, etc.).

Temperature Dependence

Magnetic properties are universal basic characteristic of a substance. They provide important information on the microscopic structure of the substance.

Magnetic characteristics can be measured by means of a vibration magnetometer; its design was taken from the book [22]. The vibration magnetometer and schematics of the installation were developed at the Physical Department, Lomonosov Moscow State University. Amended vibration magnetometers were developed at the Institute of Physics, Siberian Branch, Russian Academy of Sciences (IP SB RAS) [23, 24].

In our research on NDC materials we used a magnetometer with a superconductor magnetic field (voltage up to 60 kOe), a vibration magnetometer (field strength up to 20 kOe) [26], and a SQUID quantum interference magnetometer [5].

Among different magnetometric techniques, SQUID magnetometry has received the widest acceptance over the past years. This method is based on the effects of weak superconductivity in superconductive quan-tum interference devices (SQUIDs). It has a record-breaking high sensitivity which reaches 5×10^{-33} J/Hz (magnetic field sensitivity 10^{-13} T).

It is noteworthy that the sensitivity of the method is independent of the level of the signal to be measured, which allows reliable detection of small magnetization changes on the background of a large statistical value.

Owing to its high sensitivity, SQUID magnetometry have found application not only in the traditional

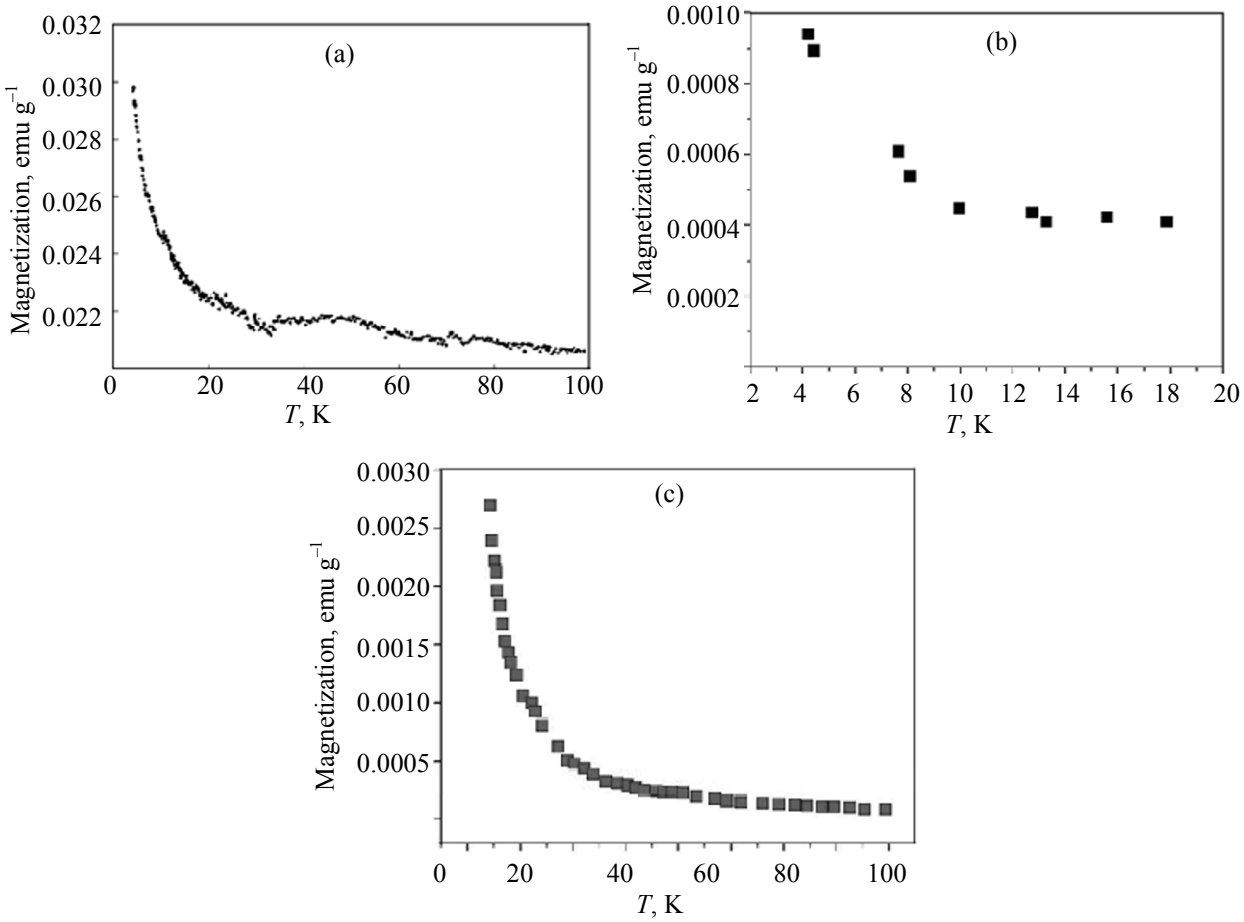

Fig. 6. Temperature dependence of magnetization for NDC samples. Sample no. in Table 3: (a) no. 2, (b) no. 10, and (c) no. 8.

field, specifically, physical experiments, but also in biomedicine, low-temperature thermometry, geophysics. This method holds great promise for studying of magnetic characteristic of substances with minor magnetic admixtures, as well as microgram-scale samples. Finally, the high sensitivity of the method makes possible measurements in very weak magnetic fields (magnetic induction $<10^{-3}$ T). In certain cases this circumstance is of key importance.

In early 1990s, the IP SB RAS developed a dc SQUID magnetometer with the following characteristics:

– absolute sensitivity 1×10^{-7} G cm^3

– dynamic range up to 5×10^{-2} G cm^3

– magnetic field range 0–2000 Oe

– working temperature range 4.2–300 K

– helium bath volume 1.2 L.

The magnetometer is equipped with an optical attachment unit which allows registration of magnetization changes under light irradiation.

The instrument showed high sensitivity, reliability, and versatility during long-term exploitation (15 years). The high sensitivity of the device allows its use for studying static magnetic properties of a wide range of objects: from strongly magnetic ferro- and ferrimagnetics to spin glasses, multilayer films, and nanostructures.

Typical temperature dependences of magnetization and reciprocal magnetic susceptibility of NDCs are shown in Figs. 6 and 7.

Field Dependences

The dependences of NDC magnetization on applied magnetic field are exemplified in Fig. 8. Evidently, a lot of such curves can be obtained for a nanodimod–pyrocarbon composite, which is explained by a fairly high sensitivity of the SQUID to iron admixtures. The concentration of admixtures was determined by the Mössbauer effect with concurrent determination of incombustible residue. It was found that is the content of iron admixtures is more than 1 wt %, a ferro-

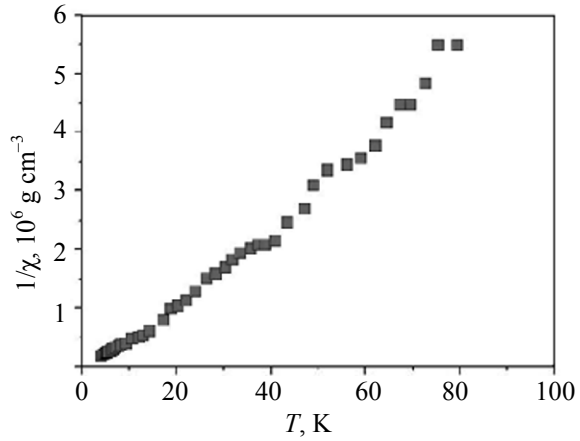

Fig. 7. Temperature dependence of reciprocal magnetic sensitivity for NDC sample no. 8 in Table 3.

magnetic hysteresis loop and Doppler shift are observed.

According to [26, 27], iron admixtures are present as individual particles quite irregularly distributed in nanodiamond samples. The carbon contents possible to obtain in NDCs are more than 99 wt %. Such materials reliably show paramagnetic invariant [9], no hysteresis loop, magnetization less than 0.01 emu g^{-1}, and complete absence of the Mössbauer effect.

The observation of an ESR signal with invariant characteristics at Fe << 0.1 wt % with simultaneous careful X-ray fluorescence analysis of the entire spectrum of admixtures in thoroughly purified NDC samples completely rules out the possibility of paramagnetism associated iron. The only source of paramagnetism in NDCs is collective Tamm electrons in nanodiamond particles [9].

The temperature dependences of magnetization were treated as follows. Magnetization data for a series of NDCs were analyzed by the Brillouin model under the assumption that the spins of electrons localized on a particle are a source of paramagnetism. By the results of this analysis (Table 1), the concentration of paramagnetic centers was estimated at ~5–6×10^{19} spin g^{-1}, which roughly corresponds to 3–10 free electron spins (electrons) per particle. The fitting results are listed in Tables 3 and 4. The impression that the data in Tables 3 and 4 contradict to each other is associated with the fact that we used different parts of a single process sample having nonuniform distribution of iron clusters.

DISCUSSION

The model of zone structure of NDCs, possible Brillouin zones in nanodiamond, and Fermi surface in NDCs are discussed in the paper devoted to the optical properties of NDCs, which is published in this journal issue.

Theoretical analysis of the particle size dependence of small-sized electron-vibrational structures associated with vibrations of surface electronic states predicts

Table 3. Results of magnetic measurements for NDC samples[a]

Sample no.	γ, %	*H*, Oe	*T*, K	Doped composite	M_{ferro}, emu g^{-1}	*N*, spin g^{-1}	*N*/*N*_m	*g*-factor	spin	χ_Σ
1	0	mes.	4.2	Fe[b]	0.05	3.00E+19	1600	4.4	0.5	4.37E-06
2	10	mes.	4.2	Fe	0.1	5.46E+19	835.16	2	0.5	–1.58E-06
3	20	mes.	4.2	Fe	0.1	5.81E+19	719.80	2	0.5	–2.14E-06
4	20	500	mes.	Cr	–	4.50E+19	261.38	2	0.5	–2.40E-06
5	30	mes.	4.2	Fe	0.08	5.46E+19	706.67	2	0.5	–1.55E-06
6	40	mes.	4.2	Fe	0.07	6.60E+19	543.12	2	0.5	–2.00E-06
7	40	mes.	4.2	Fe	0.04	6.95E+19	515.77	2	0.5	–2.33E-06
8	40	500	mes.	S	–	3.60E+19	995.72	2	0.5	–1.20E-07
9	50	mes.	2	Fe	–	2.00E+20	167.28	2	0.5	1.52E-05
10	60	500	mes.	SiO_2[c]	–	9.26E+18	3388.28	2	0.5	4.30E-07

[a] (γ) Pyrocarbon fraction (wt %) per 100% diamond mass; (mes.) measured parameter: field *H* or temperature *T*, (M_{ferro}) ferromagnetic saturation magnetization, (*N*) number of paramagnetic spins per sample, (*N*/*N*_m) number of carbon atoms per 1 spin, (*g*-factor) Lande *g*-factor, and (χ_Σ) magnetic susceptibility. [b] Weight fraction of Fe < 0.4% in all samples, except for no. 1, where Fe < 4.3 wt %. [c] (NDC) Composite in which nanodiamond is completely replaced by SiO_2.

Table 4. Results of treatment of the temperature dependences of magnetization for NDC samples[a]

Sample no.	Diamond, g	Pyrocarbon, g	Spin/g NDC	Magnetic susceptibility	CSF diameter, nm	Carbon atoms per one spin	Spin/diamond particle
0	1.00	0.00	3.00×10^{19}	4.37×10^{-6}	5.25	5112	3.0
1	0.91	0.09	5.46×10^{19}	-1.58×10^{-6}	4.96	4567	5.5
2	0.83	0.17	5.81×10^{19}	-2.14×10^{-6}	5.26	5130	7.1
3	0.77	0.23	5.46×10^{19}	-1.55×10^{-6}	5.38	5365	7.6
4	0.71	0.29	6.60×10^{19}	-2.00×10^{-6}	5.59	5787	10.6
8	0.56	0.44	6.58×10^{19}	-3.85×10^{-6}	4.81	4295	10.1

[a] Approximation by the Brillouin model, using the coherent scattering fields (CSF) obtained from the X-ray scattering spectra.

some phenomena (zero magnetic and Hall resistances) [23], which were observed in NDC semiconductors [7, 10] in insufficiently sensitive magnetic measurements and in low electric fields. The performed experiments suggest that 1D and 2D electron-vibrational states in NDCs are responsible for the mechanism of hopping conductivity in the bulk of diamond particles linked to pyrocarbon. The NDC material is a narrow-band *p*-type semiconductor and, according to the present classification [19], it is described by the Lifshitz model [28], in which the mechanism of localization of wave functions is quite different from those in the Anseson and Mott models [18, 19].

The decrease of specific conductivity typical of semiconductors has no trivial explanation in the case of nanodiamond. In coarse crystals, electrons do not enter the conductivity zone, where they would form charge carriers (electrons or holes). Why we observe an increase in the number of charge carries or even a change of sign of charge carriers in the nanocomposite at elevated temperatures?

We also propose to relate the observed dependence of electrical conductivity on temperature, namely, decrease of resistance with increasing temperature, to the localization of electrons on the nanodiamond surface. When excited, these electrons are ejected from the crystal to the upper level of the valence zone, which, in view of the small size of nanodiamond particles, is a surface level, and it is much remote from the main zone both in energy and in localization.

We performed a series of calculations to demonstrate the phenomenon of excited electron ejection onto nanocrystal surface. The surface localization facilitates electron transport between particles and explains the observed dependences.

In fact, nanoparticles associate with each other to form a solid openwork phase with pyrocarbon tethers. As a result, a certain large surface is formed, and the holes that appear when electrons enter the zone of surface state can move along this surface.

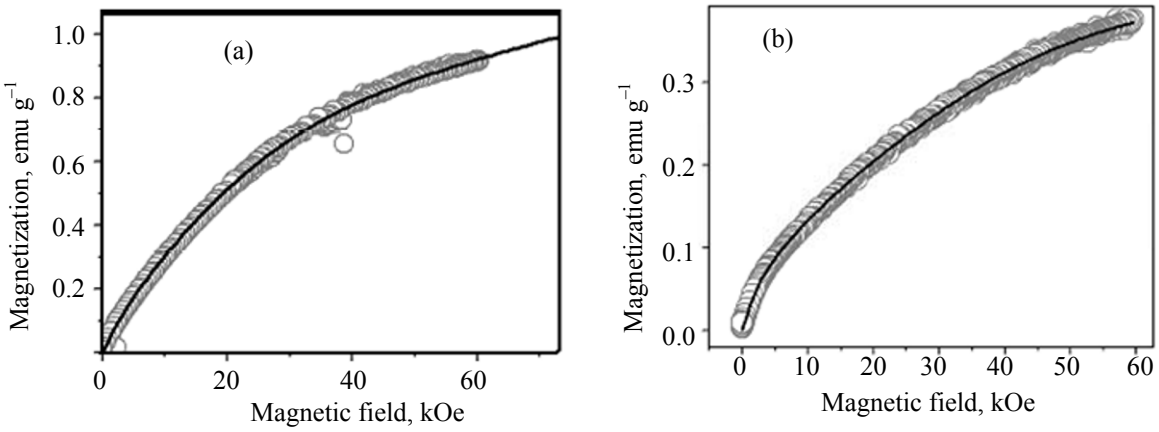

Fig. 8. Magnetization curves for NDC samples (a) no. 1 and (b) no. 7 in Table 3.

Note that the predicted change of the sign of charge carriers and, probably, evidence to be obtained in future, imply that the ratio between holes and surface electrons may change to form, in a certain moment, a gas of surface electrons moving over the inner openwork surface of the composite (this phenomenon was predicted by Tamm long ago but have not yet discovered until now). Probably, this is just due to a large inner surface of nanocomposites, the crystal surface conductivity makes a considerable contribution. We could obtain convincing experimental evidence for this explanation.

Spin conductivity should also not be excluded, which is consistent with magnetic susceptibility data.

The paramagnetism of nanodiamond and its composites, too, can be explained in terms of surface electronic states.

In the case of a coarse crystal, the electrons went out on the surface on the excitation from the valence to subsurface zone move along the surface and do not localize in three dimensions, which is required for the manifestation of spin paramagnetism. When it comes to nanocrystals, excited electrons move along the surface of a nanoparticle and localize within the nanoparticle limits (~ 5 nm). Such a localization area compares with that on a defect of crystal lattice and may well explain the existence of free spins in the nanocomposite with the carbon content of 99.9 wt %. Probably, because the localization area is as small as ~ 5 nm, the *g*-factor of such spins, observed in the ESR spectra, slightly differs from the *g*-factor of free electron [9].

Fitting the experimental data by the Brillouin function showed that each particle contains about ten effective localized spins of surface electrons. Therefore, the composite conductivity can also be associated with spin interactions between electrons localized and bound on the nanoparticle surface, which, too, does not contradict the observed temperature dependence of conductivity: As the temperature increases, the number of spins on the nanoparticle surface increase, thereby enhancing spin–spin interaction.

Collective excitations in NDCs and correlation of the wave functions of diamond particles, pyrocarbon, and pores are the principal processes responsible for the unusual and completely reproducible electrical and magnetic properties of NDC materials. The results in [26, 27] provided independent evidence for our views and for the reliability of our measurements of the electrical and magnetic characteristics of the composites of nanodiamond, pyrocarbon, and nanopores.

To conclude, we would like to note that NDC semiconductors are used as cold cathodes and substrates for growing nanodiamond films [4–6, 12, 13].

REFERENCES

1. Gordeev, S.K., Zhukov, S.G., et al., *Inorg. Mater.-Engl. Tr.,* 1995, vol. 31, pp. 434–438.
2. Gordeev, S.K., *Nanostructured Carbon for Advanced Applications*, Benedek, G., Ed., Dordrech: Kluwer, 2001, p. 71.
3. Gordeev, S.K., Zhukov, et al., US Patent 6 083 614, 2000; RF Patent 95116683, 1995.
4. Ralchenko, V., Karabutov, A., et al., *Diam. Relat. Mater*., 1999, vol. 8, pp. 1496–1501.
5. Vlasov, A.V., Ralchenko, V.G., et al., *Diam. Relat. Mater*., 2000, vol. 9, pp. 1104–1109.
6. Karabutov, A.V., Frolov, V.D., et al., *J. Vac. Sci. Technol*., 2001, vol. B19, no. 3, pp. 965–970.
7. Gordeev, S.K., Belobrov, P.I., et al., *Microcrystalline and Nanocrystalline Semiconductors-2000, MRS Proc.*, Cambridge: Cambridge Univ. Press, 2001, vol. 638, F14.16.1-6.
8. Peng, J. L., Bulcock, S., et al., *Int. J. Modern Phys. B,* 2001, vol. 15, no. 31, pp. 4071–4085.
9. Belobrov, P.I., Gordeev, S.K., et al., *Dokl. Ross. Akad. Nauk*, 2001, vol. 379, no. 1, pp. 38–41.
10. Belobrov, P.I., Kiselev, N.I., et al., *Proc. 12th Int. Symp. on Thin Films in Electronics*, Kharkov, Ukraine, 2001, pp. 38–42.
11. Belobrov, P.I., Bursill, L.A., et al., *Appl. Surf. Sci*., 2003, vol. 215, no. 1–4, pp. 169–177.
12. Karabutov, A.V., Gordeev, S.K., et al., *Diam. Relat. Mater*., 2003, vol. 12, no. 10–11, pp. 1710–1716.
13. Karabutov, A.V., Ralchenko, V.G., et al., *J. Vac. Sci. Technol*., 2003, vol. B21, pp. 597–602.
14. Belobrov, P.I., *Vysokie tekhnologii v promyshlennosti Rossii* (High Technologies in Russian Industry), Moscow: Tekhnomash, 2003, pp. 235–269.
15. Ostrovidova, G.U., Makeev, A.V., et al., *Mater. Sci. Eng.,* 2003, vol. C 23, no. 3, pp. 377–381.
16. Kulova, T.L., Evstefeeva, Yu.E., et al., *Phys. Solid State*, 2004, vol. 46, no. 4, pp. 726–728.
17. Gordeev, S.K. and Korchagina, S.B., *Sverkhtverd. Mater*., 2004, vol. 6.
18. Shklovskii, B.I. and Efros, A.L., *Elektronnye svoistva legirovannykh poluprovodnikov* (Electronic Properties of Doped Semiconductors), Moscow: Nauka, 1979.
19. Mott, N.F. and Davis, E.A., *Electronic Processes in Non-crystalline Materials*, Oxford: Clarendon, 1979, 2nd ed.

20. Bonch-Bruevich, V.L. and Morozov, A.G., *Vvedenie v elektronnuyu sistemu neuporyadochennykh poluprovodnikov* (Introduction in the Electronic System of Disordered Semiconductors), Moscow: Mosk. Gos. Univ., 1972.
21. Lifshits, I.M. and Pekar, S.M., *Usp. Fiz. Nauk*, 1955, vol. 26, no. 4, p. 556.
22. Chechernikov, V.I., *Magnitnye izmereniya* (Magnetic Measurements), Moscow: Mosk. Gos. Univ., 1969, 2nd ed.
23. Balaev, A.D., Boyarshinov, Yu.B., Karpenko M.M., and Khrustalev, B.P., *Pribory Tekh. Eksp*., 1985, no. 3, pp. 167–168.
24. Velikanov, D.A. and Yurkin, G.Yu., *Vestn. Krasnoyarsk. Gos. Univ. (Fiz.-Mat. Nauki),* 2006, vol. 9, pp. 48–53.
25. Velikanov, D.A., RF Patent no. 2246119, *Byull. Izobret*., 2005, no. 4.
26. Levin, E.M., Fang, X.W., et al., *Phys. Rev*., 2008, vol. B77, p. 054418.
27. Fang, X.W., Mao, J.D., et al., *J. Am. Chem. Soc*., 2009, vol. 131, no. 4, pp. 1426–1435.